Water as a Probe of the Colloidal Properties of Cement

LANGMUIR

Invited Feature Article

pubs.acs.org/Langmuir

Water as a Probe of the Colloidal Properties of Cement

Francesca Ridi,[†] Monica Tonelli,[†] Emiliano Fratini,*[,†] Sow-Hsin Chen,[‡] and Piero Baglioni*[,†]

[†]Department of Chemistry "Ugo Schiff" and CSGI, University of Florence, via della Lastruccia 3-Sesto Fiorentino, I-50019 Florence, Italy

[‡]Department of Nuclear Science and Engineering, Massachusetts Institute of Technology, Cambridge, Massachusetts 02139, United States

ABSTRACT: Cement is produced by mixing mineral phases based on calcium silicates and aluminates with water. The hydration reaction of the mixture leads to a synthetic material with outstanding properties that can be used as a binder for construction applications. Despite the importance of cement in society, for a long time, the chemical reactions involved in its hydration remained poorly understood as a result of the complexity of hydration processes, nanostructure, and transport phenomena. This feature article reviews the recently obtained results using water as a probe to detail the essential features in the setting process. By examining the peculiar physicochemical properties of water, fundamental information on the evolving inorganic colloid matrix can be deduced, ranging from the fractal nanostructure of the inorganic silicate framework to the transport phenomena inside the developing porosity. A similar approach can be transferred to the investigation of a plethora of other complex systems, where water plays the main role in determining the final structural and transport properties (i.e., biomaterials, hydrogels, and colloids).

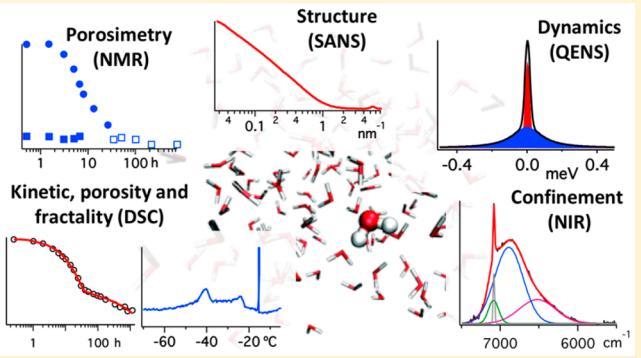

1. INTRODUCTION

The discovery of the pozzolanic reaction of volcanic materials mixed with lime and water was boasted as one of the most revolutionary innovations in history. Before the Romans, other ancient civilizations used nonhydraulic binders to build long-lasting structures such as the Great Wall in China and the Egyptian pyramids. The incredible benefits related to the addition of pozzolan to lime were the ability to set without the presence of carbon dioxide, even under water, and the impressive increase in mechanical properties. These characteristics enabled the construction of the renowned Roman aqueducts, bridges, and many other architectural structures that enormously contributed to the expansion of the Roman Empire. In modern times, three fundamental developments improved the Roman recipe for cement: the introduction of gypsum that avoids flash setting; the higher temperatures used to fire the raw materials, allowing for a more rapid setting process; and the advancement of the grinding process to increase the specific surface area available to hydration, which improves the setting process. With these changes, at the end of the XVIII century, modern Portland cement was finally formulated, and that original recipe (with few refinements) is still the most used hydraulic binder for building purposes.[1]

Cement is a complex solid that is both structurally and chemically heterogeneous. The chemical and mineralogical composition of cement formulations is variable, depending on the composition of the raw materials extracted from quarries and on the addition of extra components aimed at tuning its reactivity. With the advancement in technical knowledge, the ordinary Portland cement composition has been modified, producing several types of cements with different properties, to match specific applications. Today, a plethora of hydraulic cements are known and categorized. A summary of the most relevant is reported in Table 1. The compositions and properties of these systems are very different to cover very different applications ranging from building materials[2,3] to cement for biomedical purposes such as bone repair and orthodontics.[4] Currently, magnesium-based cements are suited for specialist applications to take advantage of their potential for CO_2 emission reduction. However, the high cost of the raw materials and the final pH not sufficiently high to passivate steel reinforcing bars limit their use and the possibility of replacing ordinary Portland cements.[3] Considering the field of cements for structural applications, magnesium silicate cement is an emerging material that finds application in the encapsulation of problematic radioactive wastes.[5−7] In addition, magnesium silicate cement is significant from a physicochemical point of view. Specifically, upon contact with water, it develops a hydrated phase (magnesium silicate hydrate, M−S−H) that is analogous to calcium silicate hydrate (C−S−H), the main binder of Portland cement. Therefore, cation substitution produces significant modifications in both the properties and structure of the hydrated phase.[8,9]

Water is one of the initial components of a cement paste and is progressively consumed during the development of the hydration products during the curing process. Therefore, the observation

Received: July 3, 2017
Revised: October 13, 2017
Published: October 16, 2017

DOI: 10.1021/acs.langmuir.7b02304
Langmuir XXXX, XXX, XXX−XXX

Table 1. Classification of Hydraulic Cements Based on Their Applications and Some of Their Main Hydration Reactions

construction and building applications		biomedical applications[10]	
material	main hydration reactions	material	main hydration reactions
Portland cement	$Ca_3SiO_5 + (1.3 + x)H_2O \rightarrow (CaO)_{1.7}SiO_2(H_2O)_x + 1.3Ca(OH)_2$	calcium phosphate	apatitic cements: $3\alpha\text{-}Ca_3(PO_4)_2 + H_2O \rightarrow Ca_9(PO_4)_5HPO_4OH$
	$Ca_2SiO_4 + (0.3 + x)H_2O \rightarrow (CaO)_{1.7}SiO_2(H_2O)_x + 0.3Ca(OH)_2$		brushite-based cements: $\beta\text{-}Ca_3(PO_4)_2 + Ca(H_2PO_4)_2H_2O + 7H_2O \rightarrow 4CaHPO_42H_2O$
	$2Ca_3Al_2O_6 + 12H_2O \rightarrow (CaO)_3Al_2O_3(H_2O)_6$		$\beta\text{-}Ca_3(PO_4)_2 + H_3PO_4 + 6H_2O \rightarrow 3CaHPO_42H_2O$
	$Ca_3Al_2O_6 + 3CaSO_4{\cdot}(H_2O)_2 + 26H_2O \rightarrow (CaO)_6Al_2O_3(SO_4)_3(H_2O)_{32}$		
Portland cement blends	$Ca_3SiO_5 + (1.3 + x)H_2O \rightarrow (CaO)_{1.7}SiO_2(H_2O)_x + 1.3Ca(OH)_2$	calcium sulfate	$CaSO_4{\cdot}0.5H_2O + 1.5H_2O \rightarrow CaSO_4{\cdot}2H_2O$
	$Ca_2SiO_4 + (0.3 + x)H_2O \rightarrow (CaO)_{1.7}SiO_2(H_2O)_x + 0.3Ca(OH)_2$		
	$2Ca_3Al_2O_6 + 12H_2O \rightarrow (CaO)_3Al_2O_3(H_2O)_6$		$CaSO_4 + 2H_2O \rightarrow CaSO_4{\cdot}2H_2O$
	$Ca_3Al_2O_6 + 3CaSO_4{\cdot}(H_2O)_2 + 26H_2O \rightarrow (CaO)_6Al_2O_3(SO_4)_3(H_2O)_{32}$		
magnesium phosphate cements	$2MgO + 2NH_4H_2PO_4 + 10H_2O \rightarrow 2NH_4MgPO_4\,6H_2O$	calcium silicate	$Ca_3SiO_5 + (1.3 + x)H_2O \rightarrow (CaO)_{1.7}SiO_2(H_2O)_x + 1.3Ca(OH)_2$
magnesium silicate hydrate cements	$xMgO + yH_2O + SiO_2 \rightarrow (MgO)_x(SiO_2)(H_2O)_y$	magnesium phosphate	$2\,MgO + 2NH_4H_2PO_4 + 10H_2O \rightarrow 2NH_4MgPO_4\,6H_2O$
			$Mg_3(PO_4)_2 + (NH_4)_2HPO_4 + 15H_2O \rightarrow 2\,MgNH_4PO_4{\cdot}6H_2O + MgHPO_4{\cdot}3H_2O$
magnesium oxychloride (Sorel) cements	$3MgO + MgCl_2 + 11H_2O \rightarrow 3\,Mg(OH)_2{\cdot}MgCl_2{\cdot}8H_2O$		
calcium sulfoaluminate cements	$(CaO)_4(Al_2O_3)_3(SO_3) + CaSO_4 + 38H_2O \rightarrow (CaO)_6Al_2O_3(SO_3)_3(H_2O)_{32} + 4Al(OH)_3$		
alkali-activated cements[10−12]	$CaO{-}SiO_2{-}MgO{-}Al_2O_3 + H_2O$ (activated with NaOH) $\rightarrow (CaO)_ySiO_2(H_2O)_x + (Mg_6Al_2CO_3(OH)_{16}{\cdot}4H_2O) + CaCO_3$ + AFm phases		

of the physicochemical properties of water during hydration allows monitoring of the reaction kinetics and structural/dynamical features that are difficult to investigate by examining the large number of products formed during the setting process. The chemical reactions that form hydrated binding phases start with a dissolution process, followed by the nucleation and growth of hydrated phases, and continue until the rate of the reaction is limited by the diffusion of water into the growing phases. These two latter stages are responsible for the final cement properties. Furthermore, cement is an exemplary system because most of the characterization methods detailed in this feature article can be applied to study different microporous and mesoporous water-containing materials to obtain information on their properties. In the following paragraphs, we will outline the major results achieved using a multitechnique approach to monitor cement characteristics at different length and time scales using water as an in situ probe.

2. HYDRATION KINETICS

The hydration kinetics have a direct impact on the evolution of the hydrated cement microstructure, which in turn influences the mechanical properties and durability of the concrete, affecting important characteristics such as strength, elastic moduli, toughness, diffusivity, and permeability to liquids and gases.[13] The complex reactions taking place between the anhydrous phases and water can be considered to be the main cause of the setting and hardening of cement pastes, and because of their exothermic nature, the hydration process is usually monitored using calorimetry, such as heat of solution calorimetry, semiadiabatic−adiabatic calorimetry, and isothermal conduction calorimetry (IC). From an industrial point of view, IC is probably the most used technique to access the hydration kinetics in the cement research field. However, this approach presents some drawbacks because the hydration process can be followed only during the early stage of hydration. A few days after mixing, the evolved heat becomes too low to be distinguished from the instrumental baseline, which prevents the use of IC in the case of slowly curing cement formulations, such as those containing retarding agents. To overcome this limit, we proposed an alternative method based on differential scanning calorimetry (DSC),[14,15] where the evolution of unreacted water can be quantified in terms of a free or freezable water index (FWI).[14,16] In this approach, cement pastes are periodically frozen at −60 °C and then melted at a constant rate. Figure 1 shows the decrease in time of the melting peak of the free, still unreacted, water for a Portland cement paste.

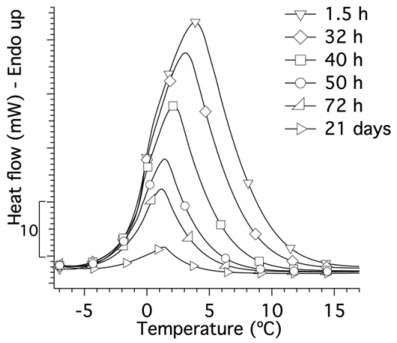

Figure 1. Evolution of the melting enthalpy of water during the hydration of a Portland cement sample (w/c = 0.4).

The ice melting peak is integrated to extract the melting enthalpy ΔH_{exp} of water and to calculate the FWI

$$\mathrm{FWI} = \frac{\Delta H_{exp}}{\phi_w \Delta H_{theor}} \quad (1)$$

DOI: 10.1021/acs.langmuir.7b02304
Langmuir XXXX, XXX, XXX−XXX

where ϕ_w is the original weight fraction of water in the paste and ΔH_{theor} is the theoretical melting enthalpy of water (333.4 J/g). In the original paper,[14] it was proven that FWI results are not affected by freeze−thaw damage expansion taking place during the DSC measurements.

Moreover, some of the authors[15] showed that hydration kinetics obtained by DSC (see, for example, Figure 2B) fully agree with those achieved from the IC technique on the very same cement paste (Figure 2A). Because DSC is based on discrete measurements, it is not limited by the evolved heat or baseline stability allowing the acquisition of data until the very end of the hydration process. Similar to IC, the DSC technique is able to capture the effect of parameters such as the water/cement ratio or temperature on the hydration kinetics.

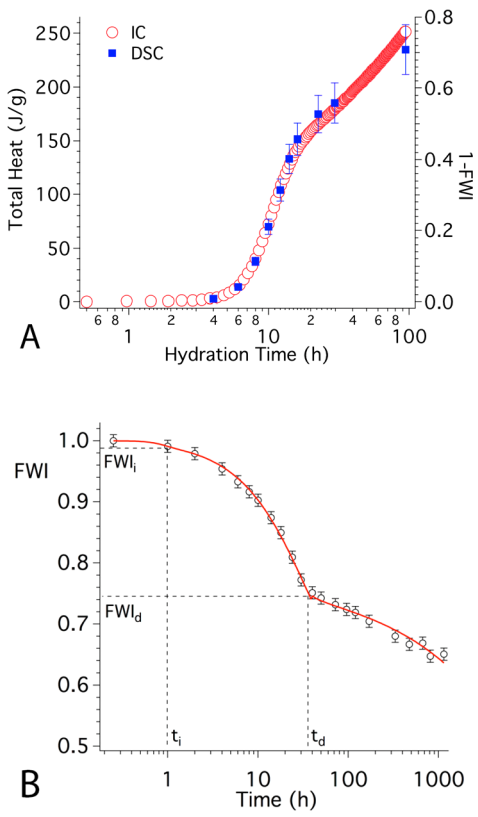

Figure 2. (A) Comparison between DSC and IC data monitoring of the hydration process of a tricalcium silicate paste (w/c = 0.4). Reproduced with permission from ref 15. (B) Hydration kinetics of a MgO/SiO_2 paste reported as FWI vs time. Black markers represent the experimental data; the red line represents the global fitting curves according to the BNGM + diffusional model. Adapted with permission from ref 28.

Kinetic analysis was used to obtain information on activation energies and rate constants of the developing hydrated phases. The hydration of cement powders is a complex multistage process with a well-known scheme: an initial hydration process, when the wetting of highly hygroscopic particles occurs; an induction period, when the reaction is quiescent; an acceleration period, when the nucleation and growth processes greatly increase the rate of the hydration reaction and the formation of several colloidal phases; a deceleration period; and finally, a diffusional period, where the reaction proceeds at a slower rate and the rate-limiting process is the diffusion of water through the hydrated products toward the anhydrous cores.[11,15,17,18] In past decades, the nucleation and growth stage taking place during the hydration of tricalcium silicate (C_3S) was modeled using Avrami-Erove'ev (AE) kinetic law[19−22] to extract the rate constants of the processes. In this framework, the DSC method was applied to investigate the effect of some of the most used cement additives, using the AE law for the acceleration period and a three-dimensional diffusion equation for the final part of the FWI curve.[16] More recently, some authors noted that the AE equation cannot completely explain the cement hydration process. Above all, the assumption that the probability of nucleation of the hydrating phases is the same elsewhere is not appropriate because it is commonly accepted that it occurs preferentially at the grain boundaries.[23] The boundary nucleation and growth model (BNGM) derived by Thomas overcomes this inconsistency.[24,25] This model, which was originally developed for solid-phase transformation,[26] can properly describe the process of cement hydration, even using fewer parameters than in the AE model. BNGM describes the hydration kinetics with two independent rate constants: k_B, which "describes the rate at which the surfaces become covered with hydration product" and k_G, which is the "rate at which the pore space between the particles fills in with product".[24,25] Then, the original BNGM approach developed for IC was modified to directly analyze the time evolution of FWI as accessed by the DSC protocol. In particular, an extra independent parameter was added to estimate the fraction of unreacted water, and any assumption on the hydration reaction stoichiometry was avoided. It was shown that the application of the model on kinetic profiles obtained by IC and DSC provides comparable results, which further validates the FWI approach.[15] Therefore, DSC was applied by our group to investigate the effects of particle size, temperature,[15] and additive addition[27] on the hydration reaction in cement pastes even for very long processes, such as those obtained with the so-called superplasticizing additives.

Some of the authors of this article recently proposed the application of BNGM[25] combined with a three-dimensional diffusional model to quantitatively describe the nucleation and growth processes during the hydration of the new green cements based on MgO/SiO_2 formulations.[28] Figure 2B shows the FWI vs time for the MgO/SiO_2 sample together with the best-fit curve obtained using the BNGM + diffusional combined model. The model accurately describes all three hydration periods. The curve shows the short initial induction period lasting until t_i is reached, where FWI remains ∼1; the nucleation and growth period, with a consistent decrease in FWI, which lasts up to ∼40 h; and the final diffusional period, starting at time t_d where the change in the curve slope suggests that the rate-limiting step becomes a diffusion-limited process, similar to the Portland case. These results agree with ^{1}H NMR relaxometry that follows the kinetics using the evolution of the transverse (T_2) spin relaxation time signal in MgO/SiO_2 pastes.[29]

The kinetics profiles associated with a curing cement paste simply detail the overall hydration reaction. During the different stages, the hydrated phases develop to yield the well-known porous structure, which is typical for cement systems. The characterization of the pore structure (i.e., total porosity, pore size distribution, and eventually specific surface area) is one of the key factors in the prediction of the final performances of cement. For example, it is known that a highly durable cement/concrete will have mostly gel pores (<5 nm) hydraulically isolated from each other.[30−32] However, accessing the porosity in detail is not trivial because of the complexity of the pore size distribution, which, in the case of a cement paste, ranges from a few nanometers to tens of micrometers, and even because many

DOI: 10.1021/acs.langmuir.7b02304
Langmuir XXXX, XXX, XXX−XXX

techniques require a dried sample with possible changes in the original porous structure. For these given reasons, experimental techniques that do not need a drying step (i.e., DSC, small-angle scattering, nuclear magnetic resonance, etc.) have a significant advantage with respect to all others (i.e., gas sorption, mercury intrusion, electron microscopy, etc.).

3. POROSITY AND FRACTALITY OF HYDRATING PHASES

Thermoporometry enables the characterization of a porous material, i.e., pore sizes, by analyzing the conditions of the solid−liquid phase transition of a condensate inside a porous matrix.[33] The method relies on the experimental evidence that when a pure substance is confined in nanometric cavities the equilibrium conditions of its solid, liquid, and gas phases depend on the curvature of the interface.[34] Therefore, the solidification/melting temperature of a liquid confined in a porous material changes with the size of the pores, and the energy involved in the phase transition is directly related to the pore volume, assuming that the liquid saturates all of the porosity. Furthermore, thermoporometry can also provide information on the shape of the pores by comparing the cooling and heating thermograms obtained in the temperature range from ambient to −80 °C (low-temperature differential scanning calorimetry, LTDSC).[33,35−38]

LTDSC was used to characterize the porosity of cement.[39−45] Bager and Sellevold investigated the formation of ice in mature Portland cement, evaluating the effect of different moisture contents, drying, and resaturation in the volume of large (capillary) and small pores.[39−41] Later, Bentz investigated the percolation of capillary porosity, which is of utmost importance in the transport properties and durability of cement structures.[42] More recently, our group investigated the properties of water confined in hydrating cement pastes,[43] showing that LTDSC thermograms can be fully explained considering the C−S−H microstructure, as described in Jennings' colloidal model II[46] (see next paragraph). LTDSC allows us to investigate matrixes with saturated porosity and can be used to estimate the volume of the meso/macroporosity, the depercolation threshold of capillary porosity (i.e., the separation of capillary pores due to the growth of hydrated phases or in other words the porosity whereby the volume fraction of connected pores in the cement paste decreases to zero), and the fractal dimension of hydrated cementitious samples, with results compatible with those obtained using more sophisticated techniques such as small-angle neutron or X-ray scattering. For example, an in-depth LTDSC investigation evidenced the differences in the microstructure and porosity among C_3S pastes hydrated in pure water and in the presence of organic superplasticizers (i.e., polycarboxylic backbone with grafted PEO chains) used in advanced cement formulations.[44]

The DSC heating scan, as reported in Figure 3A, shows a single hump in the −50 °C/0 °C temperature range as a direct consequence of the pore size distribution of cement microstructure spanning from the nanometer to micrometer scale. During heating, melting of the ice progressively occurs from the fractions confined in the smallest cavities to the fractions present in the largest ones, thus generating the hump. Conversely, the freezing process occurs in a discontinuous way, and the cooling scan shows specific peaks (e.g., Figure 3B). This peculiar behavior is usually attributed to the combination of homogeneous and heterogeneous freezing mechanisms. The homogeneous nucleation is an activated process where a free-energy barrier must be overcome for a critical crystallization nucleus to

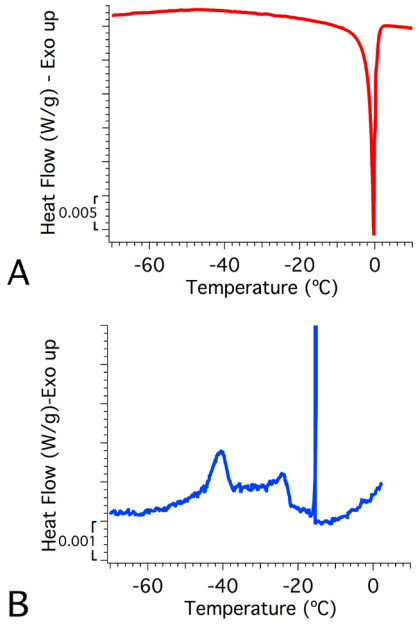

Figure 3. Heating (A) and cooling (B) scans recorded using LTDSC on a cementitious sample saturated with water. Adapted with permission from ref 44.

appear. Thus, the heterogeneous nucleation preferentially occurs because the energy required by this process is smaller. According to the molecular dynamics (MD) study on homogeneous ice nucleation,[47] at a low degree of supercooling (−20 °C < T < 0 °C), only heterogeneous nucleation is possible because of the high free energy required for the homogeneous formation of a critical nucleus (at $T \approx -15$ °C, diameter ≈ 8 nm corresponding to ∼8000 molecules). For this reason, in a saturated system, water freezes via heterogeneous nucleation even if it is confined in cavities with dimensions that are large enough to host critical nuclei isolated from the surface. Once the water in the large pores (capillary pores) is frozen, the ice remains in contact with the liquid water still present in the smaller cavities. By lowering the temperature to below −20 °C, the size of the critical cluster sensibly decreases (at $T \approx -35$ °C, diameter ≈ 3.5 nm corresponding to ∼600 molecules), and the nucleation free energy barrier decreases, making the homogeneous process likely to occur. Under these conditions, both the homogeneous and heterogeneous nucleation mechanisms become accessible at comparable rates. Then, freezing will occur in the pores whose dimensions can host a critical ice cluster that is stable at that temperature. However, the appearance of peaks in the cooling curve indicate that the process starts at the pore entrance, where the liquid water is in contact with the surrounding ice, which is a preferential site for the nucleation. The dimensional range of these freezing pores must be comparable to the size of their entrance because, for the reasons given before, the water in larger pores is already frozen at this stage, and the smaller pores cannot host a critical ice nucleus. In the case of cement pastes, the developing phases originate from three classes of nanometric porosities on top of the capillary porosity. According to Jennings' colloidal model II,[46] these are named the interlayer lamellar porosity (IGP, <1 nm), small gel pores (SGP, 1−3 nm), and large gel pores (LGP, 3−12 nm). The water inside the lamellar IGP of the primary unit cannot freeze (see paragraph on LTDSC), and thus it cannot be detected using DSC. By integrating each peak in the cooling scan (e.g., Figure 3B), the amount of water

DOI: 10.1021/acs.langmuir.7b02304
Langmuir XXXX, XXX, XXX−XXX

contained in different classes of pores (SGP, LGP, and capillary) can thus be obtained after considering the variation with temperature of the standard enthalpy of the fusion of ice.[48]

It is important to stress here that, in addition to pore size effects, the heterogeneous behavior of water crystallization at low T can also be partially ascribed to the different chemical environments experienced by the water molecules. Using the reactive force field MD method, Hou et al.[49] demonstrated that water molecules, which are confined in the nanopores of the C−S−H gel, show heterogeneity in the structure and dynamic behavior, respectively. Water molecules near the surface can react with the high-energy nonbridging oxygen atoms, producing Si−OH and Ca−OH (i.e., chemically bound water in the developing C−S−H phase). Water molecules that are approximately 1 nm away from the chemically bound water (i.e., close to the surface) have a higher arrangement, longer exchange time, and lower diffusion coefficient than bulk water because of both the strong H-bond with oxygen atoms in silicate chains and the ionic effect induced by the highly concentrated surface calcium ions.[49−51] Because of the strong hydrophilic effect from the C−S−H surface, more energy is needed for the surface-adsorbed water molecules to overcome the energy barrier to transform into ice crystals. This restriction is particularly pronounced for the water molecules confined in the nanometer pores. Moreover, the chemical composition of the C−S−H gel is also very important for influencing the thermodynamic behavior of gel pore water molecules.[52] Even if the pore size is the same, C−S−H with a lower Ca/Si ratio can reduce the diffusion rate of the interlamellar pore water to a greater extend because the protruded bridging tetrahedron has a higher tendency to disturb the transport channel that exists in the gel porosity.

The LTDSC method is useful for studying the porosity of samples containing water regardless of their composition. For example, Figure 4 shows two thermograms obtained from cementitious samples hydrated for 28 days whose composition is very different from the standard one (i.e., the water/solid ratio, w/c, is 2 instead of 0.4). In particular, Figure 4A shows the cooling scan of MgO/SiO_2: the shape of the curve indicates that, similar to C−S−H-containing matrixes, this sample has a fraction of water confined in large (capillary) pores where the liquid can freeze via heterogeneous nucleation, and another fraction that is confined in smaller pores gives rise to the large bump between −20 and −35 °C and to the sharp peak at −41 °C. Figure 4B shows Portland cement hydrated for the same time and with the same w/c: the thermogram shows that when the amount of water is high, only the capillary porosity remains, together with the porosity in the 1−3 nm range (SGP), which is a structural characteristic of the Portland-based samples. The significant difference existing between the two thermograms (in the region of −20 °C/−40 °C) can be further understood by considering the difference existing in the structure and the enclosed porosity of the two main hydration products (M−S−H and C−S−H), as we will discuss later in this article.

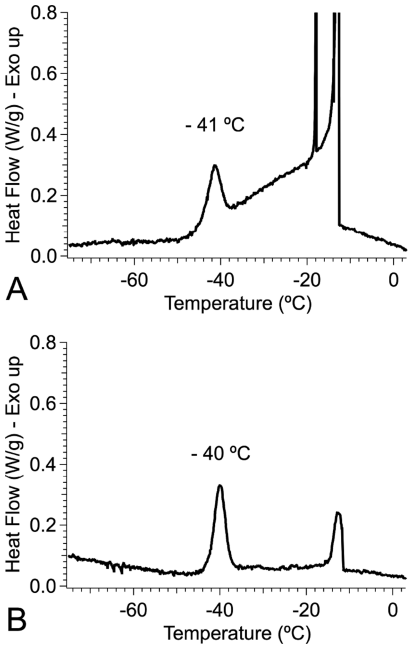

Figure 4. LTDSC cooling scans recorded on (A) MgO/SiO_2 paste and (B) Portland cement paste; both with $w/c = 2$, hydrated for 28 days and saturated with water. Adapted with permission from ref 103.

As already mentioned, the pore size distribution, $P(r)$, determines the hump in the heating part of the thermogram. Thus, in principle, it should contain information on the fractal arrangement of the cementitious matrix, which is the result of how the primary units are assembled into the volume generating the porosity of the hydrated phase. Mass and surface fractal dimensions (D_m, D_s, respectively) are usually obtained using small-angle scattering techniques, as reported in the literature for various cement pastes.[53−55] The fractal nature of porous matrixes can also be determined using DSC by relying on the fact that the melting temperature of an ice crystal confined in a pore of radius R (with $R = r - l$, where r is the radius of the pore and l is the thickness of the nonfreezable layer of water at the solid interface) is depressed by a quantity $\Delta T = T_m^0 - T_m$. Previous estimations from NMR measurements on porous glasses report a value for l of 0.5 ± 0.1 nm.[56] This is the reason that the water confined in IGP within the calcium silicate layers does not freeze, and the size of these pores is approximately 1 nm. The Gibbs−Thomson equation states that the melting temperature, T_m, and the pore radius, R, are inversely related as follows

$$T_m = T_m^0\left(\frac{1 - 2\gamma V_s}{\Delta H R}\right) \quad (2)$$

where T_m^0 is the melting temperature of an ice crystal of infinite dimension, γ is the solid−liquid interfacial tension, ΔH is the specific melting heat, and V_s is the specific volume of the solid. Considering water (i.e., $T_m^0 = 273.15$ K, $\gamma = 40 \times 10^{-3}$ N m^{-1}, $\Delta H = 334$ J g^{-1}, and $V_s = 1.02$ cm^3 g^{-1}), eq 2 becomes

$$\Delta T = \frac{68.29}{R} \quad (3)$$

with R in nanometers.

When a water-saturated porous sample, with a pore size distribution of $P(r)$, is heated from −80 °C to room temperature, the melting of the liquid confined in pores of progressively increasing dimensions occurs. Then, the heat flux registered by DSC is proportional to the incremental volume dV of the ice melting at a given temperature, T_m. If the experimental heating rate is slower than 2 °C/min, then the equilibrium conditions are satisfied[57] so that the detected heat flow is independent of the heating rate and its estimation is quantitative. The incremental pore volume per solid mass can be written as d$V = P(r)$ dr. To obtain dV, the heating signal should be normalized by the total pore volume V_p obtained by integrating the melting peak, scaled by the bulk water density value at 0 °C (0.9998 g/cm^3). According to the

DOI: 10.1021/acs.langmuir.7b02304
Langmuir XXXX, XXX, XXX−XXX

literature,[57] the heat flow, J_q, measured using DSC is related to ΔT by a scaling law consistent with the fractal nature of the systems. The porous system can be regarded as a homogeneous solid of density ρ_S, where an incremental pore volume per solid unit mass dV was used to account for the change in the bulk density of the porous sample, $\rho(r)$, as a function of the pore-filling steps.[58] Mathematically, the process is described as

$$\frac{1}{\rho(r)} = \frac{1}{\rho_S} + \int_0^r P(r)\, dr \tag{4}$$

In the fractal regime, where $a \leq r \leq \xi$, $\rho(r)$ will scale with r as follows

$$\rho(r) = \rho_S (r/a)^{D_m - 3} \tag{5}$$

where a is the characteristic dimension of the smallest repeating unit and ξ is the maximum correlation length of the fractal aggregate. Combining eqs 3 and 5,

$$dV = A(\Delta T)^{D_m - 3} \tag{6}$$

where A is the scaling factor.

Hence, D_m can be simply obtained from the fitting of the dV vs ΔT log−log plots (Figure 5). This procedure enabled us to investigate the effect of different superplasticizer on the fractality of C_3S pastes.[44] For example, Figure 5 shows the dV vs ΔT log−log plots,and the fitting lines from $\Delta T_\xi \cong 1$ K to $\Delta T_a \cong 10$ K, corresponding to pores with a radius of between 100 and 10 nm (eq 3). The size range explored by DSC is very close to what is usually measured in a standard small-angle scattering experiment.

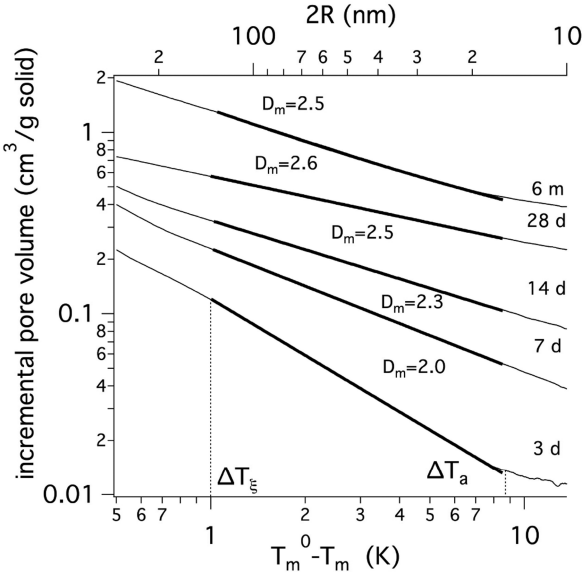

Figure 5. Incremental pore volume per solid mass as a function of the melting depression, $\Delta T = T_m^0 - T_m$ for a paste of C_3S/water during hydration. Reproduced with permission from ref 44.

As is reported in Figure 5, a C_3S/water paste ($w/c = 0.4$) has a fractal dimension that increases from 2.0 to 2.6 in the first 28 days of curing.[44] These results are in good agreement with previous SAXS investigations,[53] which reported D_m for a similar paste to vary from 1.9 to 2.8 in the same time interval. The same approach was also used on C_3S/water samples containing superplasticizers to highlight their effect on both C−S−H nanostructure and porosity. The D_m values for pastes cured for 1 month in the presence of superplasticizers resulted in lower values than in the C_3S/water case, indicating that the presence of superplasticizers causes the formation of a more open nanoscale structure with respect to a pristine sample.

Even if the exact nanostructure of the C−S−H gel is still an active topic of research, Jennings colloidal model CM-II[46,59] represents one of the best micro/nanoscale descriptions reconciling the colloidal nature of cement-based systems with a large amount of experimental data available in the literature. Very recently, CM-II was used as a starting point to work out a detailed mathematical equation that is able to depict the hierarchy of pore sizes giving rise to the fractal structure property of the C−S−H phase,[60] even including the internal structure of the globule.[61] In general, the scattering intensity distribution related to an assembly of anisotropic units can be written as

$$I(Q) = N\langle\overline{P(Q)}\rangle S(Q)_c + \text{bkg} \tag{7}$$

where N is a scaling constant considering the number density and the probe interaction of the globules, $\langle\overline{P(Q)}\rangle$ is the normalized intraparticle structure factor averaged over the distribution of the size and all possible orientations of the globules, $S(Q)_c$ accounts for the interglobule structure factor coming from the fractal arrangement corrected for the polydispersity of the system, Q is the scattering vector, and bkg is the background term. $\langle\overline{P(Q)}\rangle = \langle|F(Q)|^2\rangle$ takes into account the internal layered structure of the primary globules (i.e., $F(Q)$ is the particle form factor; in the case of C−S−H, it describe the scattering of the disklike unit).[60] If the size, orientation, and position of the basic units are uncorrelated, then $S(Q)_c = 1 + \beta(Q)[S(Q) - 1]$ with $\beta(Q) = |\langle F(Q)\rangle|^2/\langle|F(Q)|^2\rangle$. The interparticle structure factor for the fractal arrangement can be expressed as

$$S(Q) = 1 + \left(\frac{\xi}{R_e}\right)^{D_m} \Gamma(D_m + 1)\frac{\sin[(D_m - 1)\tan^{-1}(Q\xi)]}{(D_m - 1)[1 + (Q\xi)^2]^{[D_m - 1/2]}(Q\xi)} \tag{8}$$

where $R_e(3\overline{n}R^2L/4)^{1/3}$ is the equivalent radius (where $\overline{n}$ is average number of stacks in a disklike unit and R and L are defined in Figure 6) and D_m and ξ are the mass fractal and cutoff dimension of the aggregate, as already defined in the LTDSC section.

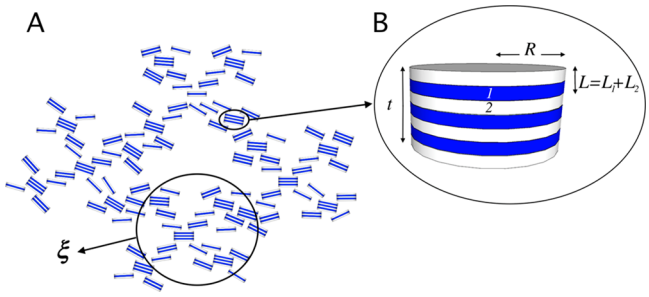

Figure 6. Interparticle (A) and intraparticle (B) structures associated with the fractal arrangement property of the disklike C−S−H units. Adapted with permission from ref 61.

This equation was used to model small-angle scattering curves (from either neutrons or X-rays) with the aim of unveiling the globule shape and size distribution as well as the fractal dimension and correlation distance characteristic of the overall arrangement in the case of the C−S−H phase. It turns out that the disklike shape of the globular unit assumed in CM-II is experimentally confirmed. This approach was used to investigate the effect of the water content[61] and of the addition of comb-shaped superplasticizers[62] on C−S−H synthetic phases.

DOI: 10.1021/acs.langmuir.7b02304
Langmuir XXXX, XXX, XXX−XXX

The decrease in the water content from 30 to 10% caused the shrinkage of the lamellar space characteristic of the IGP and concurrently an increase in the mass fractal dimension from 2.58 to 2.75, which is associated with a reduction in the average globule size from 18 to 12 nm.[61] Moreover, the addition of comb-type superplasticizers resulted in an increase in the average silicate chain length of the C−S−H building block that in the end linearly translated into an increase in dimensions of the globule.[62]

Using the same approach, some of the authors were also able to reconstruct the microstructure of synthetic M−S−H, the principal binding phase in MgO-based cements. In the case of M−S−H, the globule turned out to be spherical in shape, and more importantly, when a mixed M−S−H/C−S−H system is prepared, the two distinct morphologies are still present in the sample,[8] evidencing that these hydrates are not compatible even on the nanoscale. In both cases, a fractal arrangement of the globules is retained. However, globules pack more compactly in M−S−H but in a less extended way (ξ), resulting in a greater fractal exponent than in the C−S−H case. The intrinsic shape difference between the two types of globules in C−S−H and M−S−H gels also reflects in their morphology from submi-crometer to micrometer levels and more importantly can be a key parameter in understanding the different mechanical behavior of the MgO-based cements with respect to the better-performing CaO-based equivalent.

4. STATE OF THE WATER: NEAR-INFRARED SPECTROSCOPY, NIR

The confinement and interaction of water within the host system result in different types of water molecules being present in the cement paste (i.e., bulklike, surface-interacting or constrained, and structural). Near-infrared spectroscopy (NIR), which uses wavenumbers from 14 000−4000 cm^{-1}, provides information on the vibrational modes of stretching and bending of bonds where hydrogen is involved and, in particular, on the overtone and combination vibrations.[63] The absorption bands in the NIR region (and in particular the first overtone of the symmetric and antisymmetric O−H stretching mode of water at ∼7000 cm^{-1}) are excellent probes of the state of water because both the strength and geometry of O−H bonds affect the frequency of these peaks.[64−66] Moreover, because of the smaller extinction coefficients with respect to IR, the analysis of samples containing large amounts of water is feasible in the NIR region (i.e., saturation of the signal is not crucial). This characteristic enables the direct analysis of bulk cementitious samples with $w/c = 0.4$ or even higher. The NIR technique, probing thin layers of the samples, can provide information representative of the bulk properties only if the specimen is well-homogenized. According to the literature,[67] the absorption of water in the NIR region can be attributed to two different classes of O−H oscillators, the so-called weakly hydrogen bonded (WHB) and strongly hydrogen bonded (SHB) oscillators. The SHB oscillator has a broad absorption at lower wavenumbers, whereas the WHB oscillator is sharper and centered at higher wavenumbers. A significant increment of the WHB intensity is registered as a result of the increase in temperature[67] or the increase in the confinement effects due to a solid matrix.[65] The existence of two classes of hydrogen bonds in a C−S−H/H_2O system has also been validated by MD simulations[51] showing that the structural hydrogen bond (formed between silicate oxygen atoms and water molecules) has a longer lifetime than the hydrogen bond formed between neighboring water molecules. In the first case, the hydrogen bond is more persistent even if the interaction with the surface induces a change in the local water topology resulting in a reduction in the number of hydrogen bonds[68] (i.e., WHB in the previous notation).

When applied to a hydrating tricalcium silicate paste,[69] the NIR technique allowed the assessment of hydration kinetics by monitoring the decrease with time in the intensity of the 5000 cm^{-1} combination band: this trend follows the hydration profile as obtained using DSC (Figure 7A). The time evolution of the 7000 cm^{-1} overtone band accounts for the evolution of the two types of water coexisting in the matrix: the surface-interacting and the bulklike water. The quantification of these two species was possible by deconvoluting the 7000 cm^{-1} band into Gaussian components, as shown in Figure 7B. Figure 7C shows that the two Gaussian peaks are directly connected to the bulk water; the strongly hydrogen bonded (SHB, named β and γ) component decreases in time, and the α component, associated with the surface-interacting water, weakly hydrogen bonded (WHB) contribution, sensibly increases as a result of the developing surface area.

NIR spectroscopy is also particularly powerful in assessing the state of the confined water. This is possible by taking advantage of the temperature dependence of the NIR bands of water and ice. The behavior of the hexagonal ice NIR bands with temperature is well described in the literature, particularly for the determination of the temperature of icy regions on remote

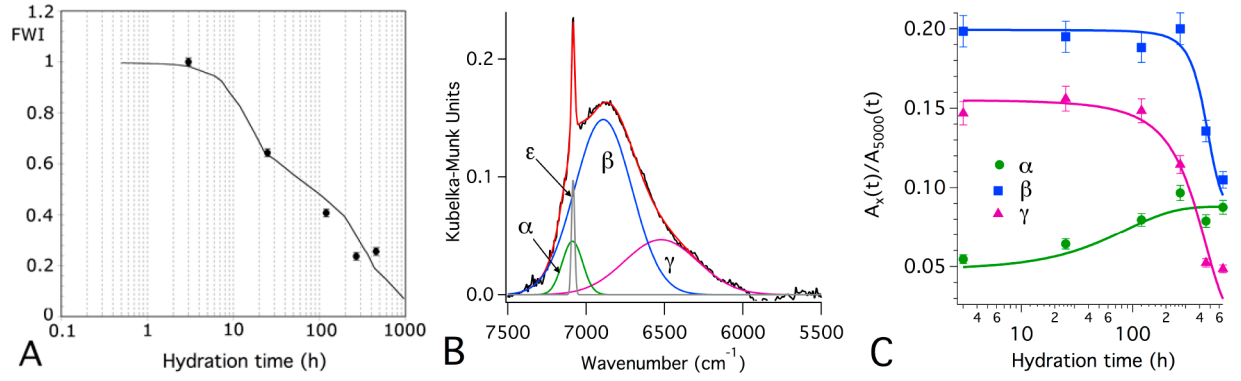

Figure 7. (A) Hydration kinetics of the C_3S + water paste, as monitored by the 5000 cm^{-1} peak area (black circles) compared to the FWI vs time curve obtained using DSC (line). (B) Deconvolution of the 7000 cm^{-1} band of the sample C_3S + water hydrated for 24 h at 20 °C: the α, β, and γ Gaussians account for the water, and the sharp ε Gaussian is linked to the OH vibrations in $Ca(OH)_2$. (C) Plot of the area vs time of the three Gaussian components describing the water contribution. Reproduced with permission from ref 69.

DOI: 10.1021/acs.langmuir.7b02304
Langmuir XXXX, XXX, XXX−XXX

planets.[70,71] The NIR spectra registered in the 20/−150 °C temperature range on a hydrated sample containing bulk water ($w/c = 0.4$) appears as shown in Figure 8A:[43] a sudden change in the shape of the 7000 cm^{-1} band occurs when liquid water freezes, with a net red shift of the entire band and the appearance of a new band centered near 6080 cm^{-1}, which is commonly considered to be a fingerprint of hexagonal ice. After a week, the trend in the spectra with temperature is similar to that shown in Figure 8B: the figure clearly shows that hexagonal ice formation is inhibited, indicating that water still present in the C_3S paste solidifies in an amorphous state. This is particularly interesting when compared to the LTDSC experiments (section 3) because it indicates that water confined in the nanometric porosity of the cement matrix is not able to crystallize but solidifies in an amorphous state.

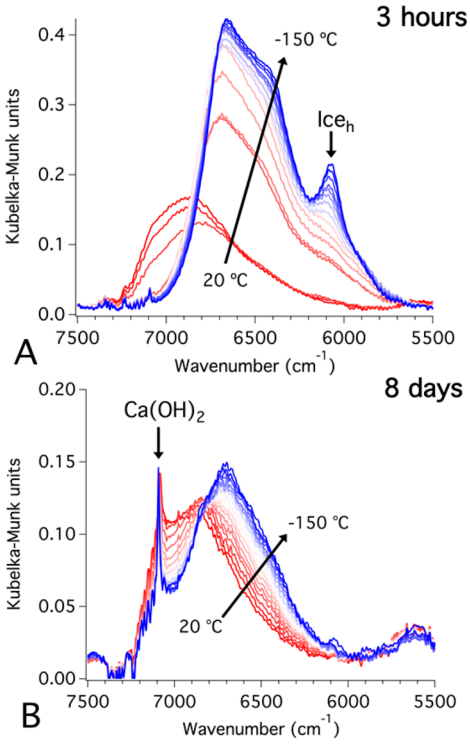

Figure 8. NIR spectra acquired from −150 to +20 °C from cement paste cured for (A) 3 h and (B) 8 days. Reproduced with permission from ref 43.

5. STATE OF THE WATER: WATER RELAXATION DYNAMICS

5.1. Quasi-Elastic Neutron Scattering. Quasi-elastic neutron scattering (QENS) is a technique especially suited for the in situ investigation of relaxation dynamics of hydrogenated species, from the picosecond to nanosecond time scale corresponding to an energy window from a few μeV to tenths of a meV.[72] In complex systems containing water, this technique allows us to characterize the actual state of the water molecules from bulk/confined to completely immobile. QENS experiments on cementitious pastes are particularly informative about water dynamics because the incoherent scattering cross section of hydrogen is 10 times larger than that of other elements constituting the cement powder (oxygen, calcium, aluminum, iron, and silicon).[21,73] Thus, the QENS signal from a cement paste is dominated by the hydrogen self-dynamics term,[74] allowing for a precise description of both the water state and the transport properties on the nanoscale. *The diffusion processes are of fundamental importance in predicting the service life (durability) of cement based systems since corrosive mechanisms involve the permeation of substances, such as aggressive ions, gases or just water, into the concrete.*[74,75]

A QENS spectrum usually contains two main contributions: an elastic and a quasi-elastic component (Figure 9A).[73,77]

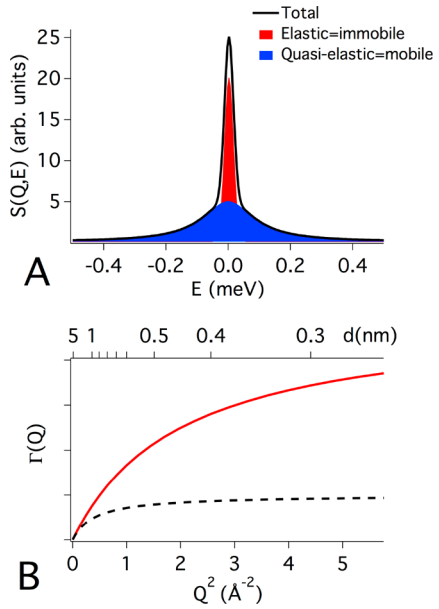

Figure 9. (A) Example of a QENS spectrum showing the two characteristic contributions: elastic and quasi-elastic, with an experimental resolution of 40 μeV. (B) Broadening of the quasi-elastic component as a function of Q^2 and the probed dimension, *d*. Passing from the continuous line (red) to the dashed line (black), the diffusion coefficient decreases, and the characteristic relaxation time increases. This is usually the evolution in time observed in a hydrating cement paste and reflects the conversion from bulk/capillary water into gel-confined water.

The elastic component is easily recognizable because it has the same width of resolution of the QENS spectrometer (and it is on the order of few tenths of a μeV). This component gathers all neutrons scattered elastically (i.e., no exchange in energy) by the nuclei that are immobile in the sample or, in other words, that relax with characteristic times longer than hundreds of ns (i.e., a time longer than the one associated with the resolution of the instrument). In the case of a cement paste, the immobile fraction accounts for the hydrogenated species (mainly chemically bound water) contained in the hydrated phases (CH, C−S−H, etc.). This quantity can be used to follow and detail the hydration kinetics in both the nucleation and growth stage and in the diffusional regime,[78] as already seen in the DSC case.

In the case of mobile atoms, the neutron−nuclei interaction results in an exchange of energy, and the QENS signal shows a broadening associated with the main relaxation processes of the sample (mainly water translational and rotational motions). In general, in the range of interest of a QENS investigation, $t > 0.1$ ps, the scattering equation for the mobile part can be generally written as $S(Q, E) = \exp(-\langle u^2\rangle Q^2/3) \otimes T(Q, E) \otimes R(Q, E)$, where the first term is the so-called Debye−Waller factor accounting for the mean square displacement of hydrogen in the O−H species, $T(Q, E)$ represents the contribution of the

DOI: 10.1021/acs.langmuir.7b02304
Langmuir XXXX, XXX, XXX−XXX

translational motion, and $R(Q, E)$ is the contribution of the rotational motion. In the case where $Q < 1$ Å^{-1}, only the translational motion is considered, which greatly simplifies the modeling of the quasi-elastic component[74,79,80] when compared to the cases where larger Q vectors are considered.[81,82] Moreover, the dependence of the broadening as a function of Q gives additional information on the type of motion (free diffusion, random jump diffusion, free diffusion in a confined geometry, etc.) allowing the calculation of the diffusion coefficient and eventually the residence times and associated jump lengths (Figure 9B). For a detailed review of the fitting models of both the mobile and immobile water fraction, the reader can refer to the literature.[83] However, current approaches tend to ignore the fact that part of the elastic signal comes from liquid water even without the presence of structural water because the Q dependence of the elastic fraction, especially at very low Q (typically $Q < 1$ Å^{-1}), contains information on the form factor of the confining volume. Very recently, to overcome this limit, a new global fitting approach has been proposed[84] where all of the QENS spectra at a given time are simultaneously modeled over a Q range covering the decay of the elastic incoherent structure factor. This novel improved analysis method can accurately extract the structural water fraction and the associated spatial information directly linked to the confinement of the matrix.

The quasi-elastic component is a key feature in disclosing the evolution of the confinement imposed by the developing C−S−H nanoporosity. Therefore, Fratini et al.[82] clearly evidenced that in the random jump diffusion approximation the average diffusion coefficient for the mobile water fraction decreases by approximately 1 order of magnitude (from 4.0×10^{-9} to 4.0×10^{-10} m^2/s) for the C_3S/H_2O model system in 2 days of curing. Not surprisingly, MD simulations for water on the surface of model C−S−H[68] resulted in an average diffusion coefficient on the order of 10^{-10} m^2/s for all surface-associated molecules, which is in agreement with our QENS investigation and with water dynamics in the ^{1}H NMR field cycling relaxation experiments.[85,86] The same decrease was evidenced by Bordallo et al.[87] by decoupling water dynamics of the capillary pores from that of the gel pores. In addition, the increase in confinement imposed by the developing inorganic matrix causes a reduction of the average jump length from 6 Å to approximately 4 Å in the first 2 days of curing.[82] Thus, the quantitative results obtained using the QENS experiment on hydrating cement pastes consist of the conversion of bulklike water (mainly contained in the capillary pores) in favor of constrained (i.e., strongly interacting with the surface, confined mainly in gel porosity) and bound water (i.e., being part of the hydration products, such as C−S−H and CH).

Recently, Bordallo et al.[88,89] disclosed very important aspects related to the hydration of cement-based systems. By following water dynamics in a 28-cured sample and in the same sample rehydrated after drying at 105 °C, they clearly found that the water reabsorbed into the dried cement paste was more mobile than the water in the pristine cured sample. This suggests that water, once reabsorbed, goes initially into capillary pores and eventually will be admitted into the gel pores only at longer times, as recently confirmed by Pinson et al. using water sorption measurements.[90] Moreover, the initial situation can also be impossible to be restored if the drying process irreversibly damaged the C−S−H nanostructure and the associated porosity.

As a matter of fact, QENS can differentiate among bound, constrained, and free water because their relaxation dynamics are quite distinct (i.e., they move differently). The advantage of this technique is twofold: it monitors the conversion of water in the hydration products and simultaneously detects the water state during the hydration of the cement paste, being able to differentiate between capillary and gel-confined water.

5.2. Porosimetry via NMR Relaxometry. The dynamics of water in a porous system can also be probed using nuclear magnetic resonance (NMR), which is noninvasive, nondestructive, and quantitative.[91] In particular, NMR relaxometry is a well-established method of characterizing pore size distributions, specific surface areas, binder phase densities, water fractions, and dynamics. This technique has been applied to calcium-based cements for decades to study the formation and characteristics of cement microstructure and to monitor the evolution of water within them. One of the main advantages of NMR experiments is that they provide highly detailed information concerning the microstructure of both crystalline and amorphous phases.[91,92]

The use of combined Carr−Purcell−Meiboom−Gill (CPMG) and quad-echo pulse sequences was recently reported in the literature as an effective method to measure and quantify all hydrogen protons in different environments such as crystalline phases, interlayer water, gel pore water, and capillary water.[91] The measurement of the transverse (T_2) and longitudinal (T_1) spin relaxation time can be used to estimate the size of the pores, to gain information on the pore network evolution during the hydration process, and to monitor the kinetics of formation of hydrogen-containing solid phases.[92−95] This technique relies on the dependence of the T_2 values of the pore water on the surface/volume ratio and on the specific surface relaxation. In the cement research field, a tool to quantitatively discriminate different populations of water has been demonstrated.[91,96−98] By assuming the fast diffusion regime,[99,100] the relationship

$$\frac{1}{T_2} \approx \frac{\varepsilon S}{V}\frac{1}{T_2^{\text{surf}}} \tag{9}$$

can be applied, in which T_2 is the measured spin−spin relaxation time, T_2^{surf} is the T_2 value for water molecules adsorbed on the surface, ε is the thickness of the adsorbed water layer, and S and V are the pore surface area and volume, respectively. Under this condition, from the experimental value of T_2, it is possible to obtain information on the S/V ratio and therefore on the pore size dimensions, distribution, and evolution in different phases.[101,102]

Similarly, this approach was further used, for the first time, with MgO/SiO_2 cements to discriminate different populations of water and to correlate their evolution with the hydration kinetics.[103] T_2 measurements were performed at different times, ranging from ∼0.5 h to 1 month, during the hydration of the investigated samples. In this study, several mixtures of Portland cement and MgO/SiO_2 were investigated, and important differences were highlighted. The two binder gel phases, magnesium silicate hydrate (M−S−H) and calcium silicate hydrate (C−S−H), showed significantly different pore size distributions. In the MgO/SiO_2 sample, three peaks were present soon after mixing with water. The peak at the shortest T_2 is due to embedded water, which broadened with increasing hydration time. The other signals were assigned to free water with different mobilities in the spaces between powder grains. The so-called less-mobile water contribution broadened, and the more-mobile water moved to shorter values and decreased with time. In the Portland cement sample, two populations of free water, less mobile and more mobile, appear soon after mixing with water. In the first 6 h, two separate peaks were present, and then they

DOI: 10.1021/acs.langmuir.7b02304
Langmuir XXXX, XXX, XXX−XXX

merged into a single signal that decreased and shifted to shorter T_2 with increases in the hydration time to up to 30 h. After 1 day of hydration, an additional signal was observed as a result of water in the gel pores and interlayer spacing, and then, at a longer hydration time, a peak assigned to water in C−S−H interlayer spaces started to be resolved, and its relative intensity increased in the first month of hydration. Figure 10 shows the

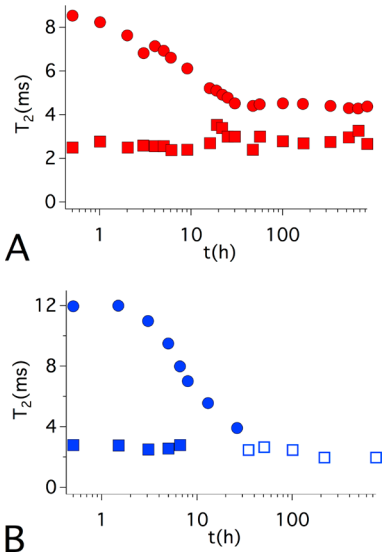

Figure 10. Evolution of hydrogen T_2 relaxation time as a function of hydration time: (A) MgO/SiO_2 and (B) Portland cement. Filled symbols (● and ■) are for the more-mobile and less-mobile free water components, and the open symbol (□) is for free water at longer hydration times, becoming water in the interhydrate spaces. Adapted with permission from ref 103.

T_2 evolution vs the hydration time for the investigated MgO/SiO_2 (Figure 10A) and Portland cement (Figure 10B). When M−S−H is the binder phase, the porous structures evolve during the entire investigated period, and the final pore distribution confirms the globular structure previously proposed in the literature.[8] However, with C−S−H as the main phase, the pore size distribution dramatically changes when this binder phase precipitates, i.e., when water remains segregated in the interlayer spaces and in gel pores.

5.3. Dielectric Relaxation. Various dielectric relaxation experiments were conducted on cement pastes and mortars. Depending on the frequency range, several relaxation processes can be followed during the hydration reaction. Typically, three components are monitored: a low relaxation occurring near 1 MHz, a medium relaxation at approximately 100 MHz, and a high relaxation in the GHz regime.[104] The main experimental evidence is that the relaxation strength of free water at high frequency (~10 GHz) decreases rapidly as the curing time passes, which enables us to follow the hydration reaction kinetics in these types of systems. The two components observed at lower frequencies (i.e., ~100 and 1 MHz) are usually distinctive of the reorientation of water constrained in the C−S−H phase.[105]

Cerveny et al.[106] studied the influence of the water level on the dielectric response of the synthetic C−S−H phase. Even in this case, three different relaxation processes related to water are present at room temperature. The effect of the temperature (110−260 K) was investigated as a function of the water level (6−15 wt %) to evidence the activation mechanism behind these relaxations. All three relaxations exhibited Arrhenius behavior at low water content (<10 wt %). With increasing water level, the process associated with water in small gel pores (medium frequency) shows a crossover from Arrhenius to super-Arrhenius (i.e., the motions become cooperative) as the water level reaches 10 wt % or in other words more than one monolayer is present. In the case of the water confined in large gel pores (high-frequency process), no crossover (from Arrhenius to super-Arrhenius) is present, and the super-Arrhenius behavior testifies to a cooperative relaxation for high water content. The two populations described agree with the findings reported using LT-NIR and DSC by some of the authors of the present paper.[43] More interesting, the crossover from Arrhenius to super-Arrhenius behavior was reported in the translational relaxation dynamics as obtained using QENS in C−S−H, M−S−H,[107] and various cement pastes.[108,109]

6. CONCLUDING DISCUSSION

The physicochemical properties of water can be a fundamental and unique resource to investigate complex porous matrixes. This feature article presented relevant results obtained on cement, which is a complex inorganic nanocomposite with structural characteristics (such as the pore size range and the dimension of the basic building block generating the fractal microstructure) that undoubtedly allow its allocation among the vast class of colloidal systems.[73] Furthermore, the number of innovative hydraulic cement formulations both for building and biomedical applications is going to increase, and the characterization of their kinetics and structural properties will become crucial for their improvement and formulation. The colloidal nature of cement suggests that the approach of using water as a probe can be extended to several other colloidal systems with very different chemical composition, where water plays a key role in the structure of the material (i.e., water is the main constituent). For example, in nonevolving systems with pores in the nanometer range, such as zeolites, clays, carbon nanotubes, or other inorganic matrixes, the thermal behavior evaluation of water is a method to infer their properties in terms of porosity, whereas the combination of QENS, NIR, NMR relaxometry, and dielectric relaxation allows one to study the translational, vibrational, and rotational motions of the confined liquid, thus evidencing the transport properties of the host material. However, biological molecules such as proteins, polysaccharides, and DNA always display behavior that is dictated by the presence of water as in the case of the plasticizing effect of water on the glass transition of biopolymers, and the study of water dynamics often yields precious information on their structure and activity. In addition, hydrogels can be successfully investigated by studying the properties of water, which directly regulates the transport phenomena of ions, molecules, and even gases through them.

■ AUTHOR INFORMATION

Corresponding Authors

*E-mail: emiliano.fratini@unifi.it.
*E-mail: piero.baglioni@unifi.it.

ORCID

Francesca Ridi: 0000-0002-6887-5108
Emiliano Fratini: 0000-0001-7104-6530
Sow-Hsin Chen: 0000-0001-6588-2428
Piero Baglioni: 0000-0003-1312-8700

DOI: 10.1021/acs.langmuir.7b02304
Langmuir XXXX, XXX, XXX−XXX

Funding

This work was performed with the financial support of Ministero dell'Istruzione, Università e Ricerca scientifica MIUR (FIR2013 project RBFR132WSM) and of Consorzio Interuniversitario per lo Sviluppo dei Sistemi a Grande Interfase, CSGI.

Notes

The authors declare no competing financial interest.

Biographies

From left to right: Sow-Hsin Chen, Piero Baglioni, Francesca Ridi, Monica Tonelli, and Emiliano Fratini

Sow-Hsin Chen, a condensed matter physicist, is a professor emeritus in the Department of Nuclear Science and Engineering at MIT (a faculty member at MIT since 1968). His main research area is thermal neutron, synchrotron X-ray, and laser light scattering spectroscopies of soft condensed matter. His recent work mainly involves molecular dynamics of various types of confined water in deeply supercooled states under high pressure, including water in MCM-41 porous silica, in cement pastes, in carbon nanotubes, and hydration water near surfaces of proteins, DNA, and RNA. He is the author of more than 450 publications in condensed matter physics.

Piero Baglioni has been a full professor of physical chemistry in the Department of Chemistry at the University of Florence since 1994 and is an MIT affiliate. He was appointed as a visiting scientist/professor by the University of Houston, the Weizmann Institute, the Collège de France, and MIT. He is the Director of CSGI, and he is on the editorial/advisory boards of several international journals and a member of the scientific board of several national and international institutions and societies. He is the author of more than 450 publications and 25 patents in the field of colloids and interfaces and a pioneer in the application of soft matter to the conservation of cultural heritage.

Francesca Ridi is a researcher in the Department of Chemistry at the University of Florence. She received her Ph.D. in chemical sciences at the University of Florence. Her research is focused on the investigation of the physicochemical processes occurring during the hydration reaction of hydraulic cements both for construction and building materials and for bone tissue engineering applications.

Monica Tonelli received her B.S. in chemistry and M.S. in chemical sciences at the University of Florence, where she is currently a Ph.D. student in chemical sciences. Her research interests include magnesium-based cements with a focus on the use of nanotubular reinforcing fibers and phosphate-based additives. She is also working in collaboration with Italcementi SpA on the physicochemical characterization of Portland-based formulations.

Emiliano Fratini is an associate professor of physical chemistry in the Department of Chemistry of the University of Florence. His research topics include multifunctional nanocomposites, novel hydrogels and organogels, water dynamics in confining matrices, new mesoporous silica scaffolds for catalysis and actives delivery, and structural and dynamical characterization of nanomaterials and soft matter.

■ ACKNOWLEDGMENTS

Ministero dell'Istruzione, Università e Ricerca scientifica MIUR (FIR2013 project RBFR132WSM), and Consorzio Interuniversitario per lo Sviluppo dei Sistemi a Grande Interfase, CSGI are acknowledged for financial support.

■ ABBREVIATIONS

NMR, nuclear magnetic resonance; CPMG, Carr−Purcell−Meiboom−Gill; LTDSC, low-temperature differential scanning calorimetry; C_3S, tricalcium silicate; PEO, poly(ethylenoxide); DSC, differential scanning calorimetry; SGP, small gel pores; LGP, large gel pores; IGP, interlamellar gel pores; FWI, free water index; AE, Avrami-Erove'ev; BNGM, boundary nucleation and growth model; NIR, near-infrared spectroscopy; WHB, weakly hydrogen bonded; SHB, strongly hydrogen bonded; QENS, quasi-elastic neutron scattering; SANS, small-angle neutron scattering

■ REFERENCES

(1) Hewlett, P. *Lea's Chemistry of Cement and Concrete*, 4th ed.; Elsevier, 1998.
(2) Khatib, J. *Sustainability of Construction Materials*; Woodhead Publishing, 2016.
(3) Walling, S. A.; Provis, J. L. Magnesia-Based Cements: A Journey of 150 Years, and Cements for the Future? *Chem. Rev.* **2016**, *116* (7), 4170−4204.
(4) Sinitsina, O. V.; Veresov, A. G.; Putlayev, V. I.; Tretyakov, Y. D.; Ravaglioli, A.; Krajewski, A.; Mazzocchi, M. Cements for Biomedical Applications. *Mendeleev Commun.* **2004**, *14* (4), 179−180.
(5) Brew, D. R. M.; Glasser, F. P. Synthesis and Characterisation of Magnesium Silicate Hydrate Gels. *Cem. Concr. Res.* **2005**, *35* (1), 85−98.
(6) Zhang, T.; Cheeseman, C. R.; Vandeperre, L. J. Development of Low pH Cement Systems Forming Magnesium Silicate Hydrate (M-S-H). *Cem. Concr. Res.* **2011**, *41* (4), 439−442.
(7) Zhang, T.; Vandeperre, L. J.; Cheeseman, C. R. Magnesium-Silicate-Hydrate Cements for Encapsulating Problematic Aluminium Containing Wastes. *J. Sustainable Cem.-Based Mater.* **2012**, *1* (1−2), 34−45.
(8) Chiang, W.-S.; Ferraro, G.; Fratini, E.; Ridi, F.; Yeh, Y.-Q.; Jeng, U. S.; Chen, S.-H.; Baglioni, P. Multiscale Structure of Calcium-and Magnesium-Silicate-Hydrate Gels. *J. Mater. Chem. A* **2014**, *2* (32), 12991−12998.
(9) Lothenbach, B.; Nied, D.; L'Hôpital, E.; Achiedo, G.; Dauzères, A. Magnesium and Calcium Silicate Hydrates. *Cem. Concr. Res.* **2015**, *77*, 60−68.
(10) Hughes, E.; Yanni, T.; Jamshidi, P.; Grover, L. M. Inorganic Cements for Biomedical Application: Calcium Phosphate, Calcium Sulphate and Calcium Silicate. *Adv. Appl. Ceram.* **2015**, *114* (2), 65−76.
(11) Taylor, H. *Cement Chemistry*; Thomas Telford Publishing: London, 1997.
(12) Wang, S.-D.; Scrivener, K. L. Hydration Products of Alkali Activated Slag Cement. *Cem. Concr. Res.* **1995**, *25* (3), 561−571.
(13) Pane, I.; Hansen, W. Investigation of Blended Cement Hydration by Isothermal Calorimetry and Thermal Analysis. *Cem. Concr. Res.* **2005**, *35* (6), 1155−1164.
(14) Damasceni, A.; Dei, L.; Fratini, E.; Ridi, F.; Chen, S.-H.; Baglioni, P. A Novel Approach Based on Differential Scanning Calorimetry Applied to the Study of Tricalcium Silicate Hydration Kinetics. *J. Phys. Chem. B* **2002**, *106* (44), 11572−11578.
(15) Ridi, F.; Fratini, E.; Luciani, P.; Winnefeld, F.; Baglioni, P. Hydration Kinetics of Tricalcium Silicate by Calorimetric Methods. *J. Colloid Interface Sci.* **2011**, *364* (1), 118−124.

DOI: 10.1021/acs.langmuir.7b02304
Langmuir XXXX, XXX, XXX−XXX

(16) Ridi, F.; Dei, L.; Fratini, E.; Chen, S.-H.; Baglioni, P. Hydration Kinetics of Tri-Calcium Silicate in the Presence of Superplasticizers. *J. Phys. Chem. B* **2003**, *107* (4), 1056−1061.
(17) Kondo, R.; Ueda, S. *Kinetics of Hydration of Cements*; Cement Association of Japan: Tokyo, 1969; Vol. *2*, pp 203−248.
(18) Jolicoeur, C.; Simard, M. Chemical Admixture-Cement Interactions: Phenomenology and Physico-Chemical Concepts. *Cem. Concr. Compos.* **1998**, *20*, 87.
(19) Brown, P. W.; Pommersheim, J.; Frohnsdorff, G. A Kinetic Model for the Hydration of Tricalcium Silicate. *Cem. Concr. Res.* **1985**, *15*, 35−41.
(20) Tarrida, M.; Madon, M.; Le Rolland, B.; Colombet, P. An in-Situ Raman Spectroscopy Study of the Hydration of Tricalcium Silicate. *Adv. Cem. Based Mater.* **1995**, *2* (1), 15−20.
(21) FitzGerald, S. A.; Neumann, D. A.; Rush, J. J.; Bentz, D. P.; Livingston, R. A. In Situ Quasi-Elastic Neutron Scattering Study of the Hydration of Tricalcium Silicate. *Chem. Mater.* **1998**, *10* (1), 397−402.
(22) Berliner, R.; Popovici, M.; Herwig, K. W.; Berliner, M.; Jennings, H. M.; Thomas, J. J. Quasielastic Neutron Scattering Study of the Effect of Water-to-Cement Ratio on the Hydration Kinetics of Tricalcium Silicate. *Cem. Concr. Res.* **1998**, *28* (2), 231−243.
(23) Garrault, S.; Behr, T.; Nonat, A. Formation of the C-S-H Layer during Early Hydration of Tricalcium Silicate Grains with Different Sizes. *J. Phys. Chem. B* **2006**, *110* (1), 270−275.
(24) Thomas, J. J. A New Approach to Modeling the Nucleation and Growth Kinetics of Tricalcium Silicate Hydration. *J. Am. Ceram. Soc.* **2007**, *90* (10), 3282−3288.
(25) Thomas, J. J.; Allen, A. J.; Jennings, H. M. Hydration Kinetics and Microstructure Development of Normal and $CaCl_2$-Accelerated Tricalcium Silicate Pastes. *J. Phys. Chem. C* **2009**, *113* (46), 19836−19844.
(26) Cahn, J. W. The Kinetics of Grain Boundary Nucleated Reactions. *Acta Metall.* **1956**, *4* (5), 449−459.
(27) Ridi, F.; Fratini, E.; Luciani, P.; Winnefeld, F.; Baglioni, P. Tricalcium Silicate Hydration Reaction in the Presence of Comb-Shaped Superplasticizers: Boundary Nucleation and Growth Model Applied to Polymer-Modified Pastes. *J. Phys. Chem. C* **2012**, *116* (20), 10887−10895.
(28) Tonelli, M.; Martini, F.; Calucci, L.; Geppi, M.; Borsacchi, S.; Ridi, F. Traditional Portland Cement and MgO-Based Cement: A Promising Combination? *Phys. Chem. Earth ABC* **2017**, *99*, 158−167.
(29) Martini, F.; Tonelli, M.; Calucci, L.; Geppi, M.; Ridi, F.; Borsacchi, S. Hydration of MgO/SiO_2 and Portland cement mixtures: a structural investigation of the hydrated phases by means of X-ray diffraction and Solid State NMR spectroscopy. *Cem. Concr. Res.* **2017**, *102*, 60.
(30) Bordallo, H. N.; Aldridge, L. P.; Desmedt, A. Water Dynamics in Hardened Ordinary Portland Cement Paste or Concrete: From Quasielastic Neutron Scattering. *J. Phys. Chem. B* **2006**, *110* (36), 17966−17976.
(31) Jacobsen, J.; Rodrigues, M. S.; Telling, M. T. F.; Beraldo, A. L.; Santos, S. F.; Aldridge, L. P.; Bordallo, H. N. Nano-Scale Hydrogen-Bond Network Improves the Durability of Greener Cements. *Sci. Rep.* **2013**, *3*, 2667.
(32) Bordallo, H. N.; Aldridge, L. P.; Fouquet, P.; Pardo, L. C.; Unruh, T.; Wuttke, J.; Yokaichiya, F. Hindered Water Motions in Hardened Cement Pastes Investigated over Broad Time and Length Scales. *ACS Appl. Mater. Interfaces* **2009**, *1* (10), 2154−2162.
(33) Brun, M.; Lallemand, A.; Quinson, J. F.; Eyraud, C. A New Method for the Simultaneous Determination of the Size and the Shape of Pores: The Thermoporometry. *Thermochim. Acta* **1977**, *21*, 59−87.
(34) Defay, R.; Prigogine, I.; Bellemans, A.; Everett, D. H. *Surface Tension and Adsorption*; Longmans Green: London, 1966.
(35) Landry, M. R. Thermoporometry by Differential Scanning Calorimetry: Experimental Considerations and Applications. *Thermochim. Acta* **2005**, *433* (1−2), 27−50.
(36) Ishikiriyama, K.; Todoki, M. Pore Size Distribution Measurements of Silica Gels by Means of Differential Scanning Calorimetry. *J. Colloid Interface Sci.* **1995**, *171* (1), 103−111.
(37) Ishikiriyama, K.; Todoki, M. Evaluation of Water in Silica Pores Using Differential Scanning Calorimetry. *Thermochim. Acta* **1995**, *256* (2), 213−226.
(38) Ishikiriyama, K.; Todoki, M.; Motomura, K. Pore Size Distribution (PSD) Measurements of Silica Gels by Means of Differential Scanning Calorimetry: I. Optimization for Determination of PSD. *J. Colloid Interface Sci.* **1995**, *171* (1), 92−102.
(39) Bager, D. H.; Sellevold, E. J. Ice Formation in Hardened Cement Paste, Part I — Room Temperature Cured Pastes with Variable Moisture Contents. *Cem. Concr. Res.* **1986**, *16* (5), 709−720.
(40) Bager, D. H.; Sellevold, E. J. Ice Formation in Hardened Cement Paste, Part II — Drying and Resaturation on Room Temperature Cured Pastes. *Cem. Concr. Res.* **1986**, *16* (6), 835−844.
(41) Bager, D. H.; Sellevold, E. J. Ice Formation in Hardened Cement Paste, Part III — Slow Resaturation of Room Temperature Cured Pastes. *Cem. Concr. Res.* **1987**, *17* (1), 1−11.
(42) Bentz, D. P. Capillary Porosity Depercolation/Repercolation in Hydrating Cement Pastes Via Low-Temperature Calorimetry Measurements and CEMHYD3D Modeling. *J. Am. Ceram. Soc.* **2006**, *89* (8), 2606−2611.
(43) Ridi, F.; Luciani, P.; Fratini, E.; Baglioni, P. Water Confined in Cement Pastes as a Probe of Cement Microstructure Evolution. *J. Phys. Chem. B* **2009**, *113* (10), 3080−3087.
(44) Ridi, F.; Fratini, E.; Baglioni, P. Fractal Structure Evolution during Cement Hydration by Differential Scanning Calorimetry: Effect of Organic Additives. *J. Phys. Chem. C* **2013**, *117* (48), 25478−25487.
(45) Sun, Z.; Scherer, G. W. Pore size and shape in mortar by thermoporometry. *Cem. Concr. Res.* **2010**, *40* (5), 740−751.
(46) Jennings, H. M. Refinements to Colloid Model of CSH in Cement: CM-II. *Cem. Concr. Res.* **2008**, *38* (3), 275−289.
(47) Sanz, E.; Vega, C.; Espinosa, J. R.; Caballero-Bernal, R.; Abascal, J. L. F.; Valeriani, C. Homogeneous Ice Nucleation at Moderate Supercooling from Molecular Simulation. *J. Am. Chem. Soc.* **2013**, *135* (40), 15008−15017.
(48) Hansen, E. W.; Gran, H. C.; Sellevold, E. J. Heat of Fusion and Surface Tension of Solids Confined in Porous Materials Derived from a Combined Use of NMR and Calorimetry. *J. Phys. Chem. B* **1997**, *101* (35), 7027−7032.
(49) Hou, D.; Zhao, T.; Ma, H.; Li, Z. Reactive molecular simulation on water confined in the nanopores of the calcium silicate hydrate gel: structure, reactivity, and mechanical properties. *J. Phys. Chem. C* **2015**, *119* (3), 1346−1358.
(50) Li, D. K.; Zhao, W. Y.; Hou, D. S.; Zhao, T. J. Molecular dynamics study on the chemical bound, physical adsorbed and ultra-confined water molecules in the nano-pore of calcium silicate hydrate. *Constr. Build. Mater.* **2017**, *151*, 563−574.
(51) Youssef, M.; Pellenq, R. J. M.; Yildiz, B. Glassy nature of water in an ultraconfining disordered material: the case of calcium− silicate−hydrate. *J. Am. Chem. Soc.* **2011**, *133* (8), 2499−2510.
(52) Qomi, M. J. A.; Bauchy, M.; Ulm, F. J.; Pellenq, R. J. M. Anomalous composition-dependent dynamics of nanoconfined water in the interlayer of disordered calcium-silicates. *J. Chem. Phys.* **2014**, *140* (5), 054515.
(53) Kriechbaum, M.; Degovics, G.; Tritthart, J.; Laggner, P. Fractal Structure of Portland Cement Paste during Age Hardening Analyzed by Small-Angle X-Ray Scattering. *Prog. Colloid Polym. Sci.* **1989**, *79*, 101−105.
(54) Livingston, R. A. Fractal Nucleation and Growth Model for the Hydration of Tricalcium Silicate. *Cem. Concr. Res.* **2000**, *30*, 1853−1860.
(55) Winslow, D.; Bukowski, J. M.; Young, J. F. The Fractal Arrangement of Hydrated Cement Paste. *Cem. Concr. Res.* **1995**, *25* (1), 147−156.
(56) Rault, J.; Neffati, R.; Judeinstein, P. Melting of Ice in Porous Glass: Why Water and Solvents Confined in Small Pores Do Not Crystallize? *Eur. Phys. J. B* **2003**, *36* (4), 627−637.
(57) Neffati, R.; Rault, J. Pore Size Distribution in Porous Glass: Fractal Dimension Obtained by Calorimetry. *Eur. Phys. J. B* **2001**, *21* (2), 205−210.

DOI: 10.1021/acs.langmuir.7b02304
Langmuir XXXX, XXX, XXX−XXX

(58) Vollet, D.; Donatti, D.; Ruiz, A. I. Comparative Study Using Small-Angle X-Ray Scattering and Nitrogen Adsorption in the Characterization of Silica Xerogels and Aerogels. *Phys. Rev. B: Condens. Matter Mater. Phys.* **2004**, *69* (6), 64202.
(59) Jennings, H. M. A Model for the Microstructure of Calcium Silicate Hydrate in Cement Paste. *Cem. Concr. Res.* **2000**, *30* (1), 101−116.
(60) Allen, A. J.; Thomas, J. J.; Jennings, H. M. Composition and Density of Nanoscale Calcium-Silicate-Hydrate in Cement. *Nat. Mater.* **2007**, *6* (4), 311−316.
(61) Chiang, W.-S.; Fratini, E.; Baglioni, P.; Liu, D.; Chen, S.-H. Microstructure Determination of Calcium-Silicate-Hydrate Globules by Small-Angle Neutron Scattering. *J. Phys. Chem. C* **2012**, *116* (8), 5055−5061.
(62) Chiang, W.-S.; Fratini, E.; Ridi, F.; Lim, S.-H.; Yeh, Y.-Q.; Baglioni, P.; Choi, S.-M.; Jeng, U.-S.; Chen, S.-H. Microstructural Changes of Globules in Calcium−silicate−hydrate Gels with and without Additives Determined by Small-Angle Neutron and X-Ray Scattering. *J. Colloid Interface Sci.* **2013**, *398*, 67−73.
(63) Siesler, H. W. *Near-Infrared Spectroscopy: Principles, Instruments, Applications*; Wiley-VCH: Weinheim, 2002.
(64) Andaloro, G.; Chiricò, P.; Guzzio, G.; Leone, M.; Palma-Vittorelli, M. B. Thermal Behavior of the near IR Absorption of H_2O and $NaClO_4$ Aqueous Solutions. *J. Chem. Phys.* **1977**, *66* (1), 335−341.
(65) Cupane, A.; Levantino, M.; Santangelo, M. G. Near-Infrared Spectra of Water Confined in Silica Hydrogels in the Temperature Interval 365−5 K. *J. Phys. Chem. B* **2002**, *106* (43), 11323−11328.
(66) Czarnik-Matusewicz, B.; Pilorz, S.; Hawranek, J. P. Temperature-Dependent Water Structural Transitions Examined by near-IR and Mid-IR Spectra Analyzed by Multivariate Curve Resolution and Two-Dimensional Correlation Spectroscopy. *Anal. Chim. Acta* **2005**, *544* (1−2), 15−25.
(67) Angell, C. A.; Rodgers, V. Near Infrared Spectra and the Disrupted Network Model of Normal and Supercooled Water. *J. Chem. Phys.* **1984**, *80* (12), 6245−6252.
(68) Hou, D.; Li, Z.; Zhao, T.; Zhang, P. Water transport in the nano-pore of the calcium silicate phase: reactivity, structure and dynamics. *Phys. Chem. Chem. Phys.* **2015**, *17* (2), 1411−1423.
(69) Ridi, F.; Fratini, E.; Milani, S.; Baglioni, P. Near-Infrared Spectroscopy Investigation of the Water Confined in Tricalcium Silicate Pastes. *J. Phys. Chem. B* **2006**, *110* (33), 16326−16331.
(70) Grundy, W. M.; Schmitt, B. The Temperature-Dependent near-Infrared Absorption Spectrum of Hexagonal H_2O Ice. *J. Geophys. Res. Planets* **1998**, *103* (E11), 25809−25822.
(71) Grundy, W. M.; Buie, M. W.; Stansberry, J. A.; Spencer, J. R.; Schmitt, B. Near-Infrared Spectra of Icy Outer Solar System Surfaces: Remote Determination of H_2O Ice Temperatures. *Icarus* **1999**, *142* (2), 536−549.
(72) Bee, M. *Quasielastic Neutron Scattering: Principles and Applications in Solid State Chemistry, Biology and Materials Science*; Adam Hilger: Bristol, 1988.
(73) Ridi, F.; Fratini, E.; Baglioni, P. Cement: A Two Thousand Year Old Nano-Colloid. *J. Colloid Interface Sci.* **2011**, *357*, 255−264.
(74) Fratini, E.; Chen, S. H.; Baglioni, P.; Bellissent-Funel, M. C. Quasi-Elastic Neutron Scattering Study of Translational Dynamics of Hydration Water in Tricalcium Silicate. *J. Phys. Chem. B* **2002**, *106* (1), 158−166.
(75) RILEM Technical Committee TC 116-PCD; *Relations between Transport Characteristics and Durability*; Hilsdorf, H., Kropp, J., Eds.; E & FN Spon: London,1995.
(76) Mindess, S.; Young, J. F.; Darwin, D. *Concrete*, 2nd ed.; Prentice Hall: Upper Saddle River, NJ, 2003.
(77) Harris, D. H. C.; Windsor, C. G.; Lawrence, C. D. Free and Bound Water in Cement Pastes. *Mag. Concr. Res.* **1974**, *26* (87), 65−72.
(78) Del Buffa, S.; Fratini, E.; Ridi, F.; Faraone, A.; Baglioni, P. State of Water in Hydrating Tricalcium Silicate Pastes: The Effect of a Cellulose Ether. *J. Phys. Chem. C* **2016**, *120* (14), 7612−7620.
(79) Fratini, E.; Chen, S. H.; Baglioni, P.; Bellissent-Funel, M. C. Age-Dependent Dynamics of Water in Hydrated Cement Paste. *Phys. Rev. E: Stat. Phys., Plasmas, Fluids, Relat. Interdiscip. Top.* **2001**, *64* (2), 20201.
(80) Fratini, E.; Chen, S. H.; Baglioni, P. Investigation of the Temporal Evolution of Translational Dynamics of Water Molecules in Hydrated Calcium Aluminate Pastes. *J. Phys. Chem. B* **2003**, *107* (37), 10057−10062.
(81) Li, H.; Zhang, L.-L.; Yi, Z.; Fratini, E.; Baglioni, P.; Chen, S.-H. Translational and Rotational Dynamics of Water Contained in Aged Portland Cement Pastes Studied by Quasi-Elastic Neutron Scattering. *J. Colloid Interface Sci.* **2015**, *452*, 2−7.
(82) Fratini, E.; Faraone, A.; Ridi, F.; Chen, S.-H.; Baglioni, P. Hydration Water Dynamics in Tricalcium Silicate Pastes by Time-Resolved Incoherent Elastic Neutron Scattering. *J. Phys. Chem. C* **2013**, *117* (14), 7358−7364.
(83) Peterson, V. K. Studying the Hydration of Cement. In *Studying Kinetics with Neutrons: Prospects for Times-Resolved Neutron Scattering*; Springer Series in Solid-State Sciences; Springer, 2010; Vol. *161*, pp 19−75.
(84) Le, P.; Fratini, E.; Zhang, L.-L.; Ito, K.; Mamontov, E.; Baglioni, P.; Chen, S.-H. Quasi-Elastic Neutron Scattering Study of Hydration Water in Synthetic Cement: An Improved Analysis Method Based on a New Global Model. *J. Phys. Chem. C* **2017**, *121*, 12826−12833.
(85) Kalinichev, A. G.; Wang, J.; Kirkpatrick, R. J. Molecular Dynamics Modeling of the Structure, Dynamics and Energetics of Mineral−water Interfaces: Application to Cement Materials. *Cem. Concr. Res.* **2007**, *37* (3), 337−347.
(86) Korb, J.-P.; McDonald, P. J.; Monteilhet, L.; Kalinichev, A. G.; Kirkpatrick, R. J. Comparison of Proton Field-Cycling Relaxometry and Molecular Dynamics Simulations for Proton−water Surface Dynamics in Cement-Based Materials. *Cem. Concr. Res.* **2007**, *37* (3), 348−350.
(87) Bordallo, H. N.; Aldridge, L. P.; Desmedt, A. Water Dynamics in Hardened Ordinary Portland Cement Paste or Concrete: From Quasielastic Neutron Scattering. *J. Phys. Chem. B* **2006**, *110* (36), 17966−17976.
(88) Jacobsen, J.; Rodrigues, M. S.; Telling, M. T. F.; Beraldo, A. L.; Santos, S. F.; Aldridge, L. P.; Bordallo, H. N. Nano-Scale Hydrogen-Bond Network Improves the Durability of Greener Cements. *Sci. Rep.* **2013**, *3*, 2667.
(89) Bordallo, H. N.; Aldridge, L. P.; Fouquet, P.; Pardo, L. C.; Unruh, T.; Wuttke, J.; Yokaichiya, F. Hindered Water Motions in Hardened Cement Pastes Investigated over Broad Time and Length Scales. *ACS Appl. Mater. Interfaces* **2009**, *1* (10), 2154−2162.
(90) Pinson, M. B.; Masoero, E.; Bonnaud, P. A.; Manzano, H.; Ji, Q.; Yip, S.; Thomas, J. J.; Bazant, M. Z.; Van Vliet, K. J.; Jennings, H. M. Hysteresis from Multiscale Porosity: Modeling Water Sorption and Shrinkage in Cement Paste. *Phys. Rev. Appl.* **2015**, *3*, 064009.
(91) Muller, A. C. A.; Scrivener, K. L.; Gajewicz, A. M.; McDonald, P. J. Use of Bench-Top NMR to Measure the Density, Composition and Desorption Isotherm of C−S−H in Cement Paste. *Microporous Mesoporous Mater.* **2013**, *178*, 99−103.
(92) Valori, A.; McDonald, P. J.; Scrivener, K. L. The Morphology of C−S−H: Lessons from ^{1}H Nuclear Magnetic Resonance Relaxometry. *Cem. Concr. Res.* **2013**, *49*, 65−81.
(93) Faure, P. F.; Rodts, S. Proton NMR Relaxation as a Probe for Setting Cement Pastes. *Magn. Reson. Imaging* **2008**, *26* (8), 1183−1196.
(94) Korb, J.-P. NMR and Nuclear Spin Relaxation of Cement and Concrete Materials. *Curr. Opin. Colloid Interface Sci.* **2009**, *14* (3), 192−202.
(95) Bortolotti, V.; Fantazzini, P.; Mongiorgi, R.; Sauro, S.; Zanna, S. Hydration Kinetics of Cements by Time-Domain Nuclear Magnetic Resonance: Application to Portland-Cement-Derived Endodontic Pastes. *Cem. Concr. Res.* **2012**, *42* (3), 577−582.
(96) McDonald, P. J.; Rodin, V.; Valori, A. Characterisation of Intra- and Inter-C−S−H Gel Pore Water in White Cement Based on an Analysis of NMR Signal Amplitudes as a Function of Water Content. *Cem. Concr. Res.* **2010**, *40* (12), 1656−1663.
(97) Pop, A.; Badea, C.; Ardelean, I. The Effects of Different Superplasticizers and Water-to-Cement Ratios on the Hydration of

DOI: 10.1021/acs.langmuir.7b02304
Langmuir XXXX, XXX, XXX−XXX

Gray Cement Using T_2-NMR. *Appl. Magn. Reson.* **2013**, *44* (10), 1223−1234.
(98) Bligh, M. W.; d'Eurydice, M. N.; Lloyd, R. R.; Arns, C. H.; Waite, T. D. Investigation of Early Hydration Dynamics and Microstructural Development in Ordinary Portland Cement Using ^{1}H NMR Relaxometry and Isothermal Calorimetry. *Cem. Concr. Res.* **2016**, *83*, 131−139.
(99) Brownstein, K. R.; Tarr, C. E. Importance of Classical Diffusion in NMR Studies of Water in Biological Cells. *Phys. Rev. A: At., Mol., Opt. Phys.* **1979**, *19* (6), 2446−2453.
(100) Halperin, W. P.; Jehng, J.-Y.; Song, Y.-Q. Application of Spin-Spin Relaxation to Measurement of Surface Area and Pore Size Distributions in a Hydrating Cement Paste. *Magn. Reson. Imaging* **1994**, *12* (2), 169−173.
(101) Gombia, M.; Bortolotti, V.; De Carlo, B.; Mongiorgi, R.; Zanna, S.; Fantazzini, P. Nanopore Structure Buildup during Endodontic Cement Hydration Studied by Time-Domain Nuclear Magnetic Resonance of Lower and Higher Mobility ^{1}H. *J. Phys. Chem. B* **2010**, *114* (5), 1767−1774.
(102) Muller, A. C. A.; Scrivener, K. L.; Gajewicz, A. M.; McDonald, P. J. Densification of C−S−H Measured by ^{1}H NMR Relaxometry. *J. Phys. Chem. C* **2013**, *117* (1), 403−412.
(103) Martini, F.; Calucci, L.; Geppi, M.; Tonelli, M.; Ridi, F.; Borsacchi, S. Monitoring the Hydration of MgO-Based Cement and Its Mixtures with Portland Cement by ^{1}H NMR Relaxometry. *Microporous Mesoporous Mater.* **2017**, doi: 10.1016/j.micromeso.2017.05.031.
(104) Hager, N. E.; Domszy, R. C. Monitoring of Cement Hydration by Broadband Time-Domain-Reflectometry Dielectric Spectroscopy. *J. Appl. Phys.* **2004**, *96* (9), 5117−5128.
(105) Miura, N.; Shinyashiki, N.; Yagihara, S.; Shiotsubo, M. Microwave Dielectric Study of Water Structure in the Hydration Process of Cement Paste. *J. Am. Ceram. Soc.* **1998**, *81* (1), 213−216.
(106) Cerveny, S.; Arrese-Igor, S.; Dolado, J. S.; Gaitero, J. J.; Alegria, A.; Colmenero, J. Effect of Hydration on the Dielectric Properties of C-S-H Gel. *J. Chem. Phys.* **2011**, *134* (3), 034509.
(107) Le, P.; Fratini, E.; Ito, K.; Wang, Z.; Mamontov, E.; Baglioni, P.; Chen, S.-H. Dynamical Behaviors of Structural, Constrained and Free Water in Calcium- and Magnesium-Silicate-Hydrate Gels. *J. Colloid Interface Sci.* **2016**, *469*, 157−163.
(108) Zhang, Y.; Lagi, M.; Fratini, E.; Baglioni, P.; Mamontov, E.; Chen, S.-H. Dynamic Susceptibility of Supercooled Water and Its Relation to the Dynamic Crossover Phenomenon. *Phys. Rev. E* **2009**, *79* (4), 40201.
(109) Li, H.; Chiang, W.-S.; Fratini, E.; Ridi, F.; Bausi, F.; Baglioni, P.; Tyagi, M.; Chen, S.-H. Dynamic Crossover in Hydration Water of Curing Cement Paste: The Effect of Superplasticizer. *J. Phys.: Condens. Matter* **2012**, *24* (6), 064108.

DOI: 10.1021/acs.langmuir.7b02304
Langmuir XXXX, XXX, XXX−XXX